



Disturbances in an initially stressed fiber-reinforced orthotropic thermoelastic medium due to inclined load

Sunita Deswal¹ · Ravinder Poonia¹ · Kapil Kumar Kalkal¹

Received: 25 August 2019 / Accepted: 6 April 2020 / Published online: 27 April 2020
© The Brazilian Society of Mechanical Sciences and Engineering 2020

Abstract

The present concept is related to the two-dimensional deformation in an initially stressed fiber-reinforced orthotropic thermoelastic model in the context of Green–Naghdi type III (GN III) theory as a result of the application of an inclined load. Normal and shear loads are assumed to be linear. The full expressions for the displacement components, temperature field and stresses are obtained by using normal mode technique. Comparisons are made in an orthotropic, transversely isotropic and an isotropic medium to illustrate the effects of fiber reinforcement on these physical quantities. The effects of initial stress, Green–Naghdi theories (type III and type II), inclination angle of load and time on the field variables are also considered.

Keywords Green–Naghdi theories · Fiber-reinforced thermoelastic composites · Orthotropic · Initial stress · Inclined load · Normal mode technique

1 Introduction

A fiber-reinforced composite is a structural material that consists of mainly three components: the fibers or the discontinuous or dispersed phase, the matrix as the continuous phase and the fine interphase region, also known as the interface. The parts made with fiber-reinforced composite materials have a higher material index than traditional materials and therefore competent to minimum mass design and have remarkable advantages such as lightweight with high strength, good corrosion resistance, rational impact resistance, dimension stability, durability and easy mold ability. Mallick [1] pointed out the applications of fiber-reinforced composites in medical science field, automotive field, defense marine, aerospace, motorsports, pipelines, pressure vessels, breathing tanks, gas cylinders, wind turbine blades, boats, architectural shapes, automobile parts, beams and girders used in roof structures, bridges and helicopter rotor shafts.

Abbas [2] showed that the mechanical behavior of many fiber-reinforced composite materials can be adequately modeled by the theory of linear elasticity for anisotropic materials. Hashin and Rosen [3] introduced the elastic moduli for fiber-reinforced composites. For the last few decades, the analysis of stress and deformation of fiber-reinforced composites has been a substantial topic in the solid mechanics. Pipkin [4] and Rogers [5] discussed a continuum theory of finite plane deformations of composites consisting of materials reinforced by strong fibers. The composite is assumed to be incompressible, and the fibers are treated as inextensible and continuously distributed. Belfield et al. [6] introduced continuous self-reinforcement at each point of an elastic medium and derived an exact solution of a boundary value problem for an annulus circumscribed by concentric circles. Singh [7] studied the plane wave propagation in a fiber-reinforced anisotropic generalized thermoelastic medium. Othman and Lotfy [8] solved a two-dimensional problem of fiber-reinforced thermoelastic medium under the effects of gravitational, rotational and magnetic fields in the context of coupled, Lord–Shulman and Green–Lindsay theories. Kalkal et al. [9] investigated the thermal disturbances in a diffusive fiber-reinforced transversely isotropic thermoelastic half-space in the context of Green–Lindsay (GL) theory. Deswal et al. [10] investigated the effects of initial stress and gravity in a fiber-reinforced transversely isotropic thermoelastic half-space with diffusion.

Technical Editor: João Marciano Laredo dos Reis.

✉ Kapil Kumar Kalkal
kapilkalkal_gju@rediffmail.com

¹ Department of Mathematics, Guru Jambheshwar University of Science and Technology, Hisar, Haryana 125001, India

Biot [11] developed the coupled theory of thermoelasticity which admits an infinite velocity of propagation for thermal signals. To remove this physically impossible phenomenon, Lord and Shulman [12] formulated the generalized thermoelasticity theory involving one thermal relaxation time. Green and Lindsay [13] developed a temperature rate-dependent thermoelasticity theory that includes two thermal relaxation times and does not violate the classical Fourier's law of heat conduction. Later on, by providing sufficient basic modifications in the constitutive equations, Green and Naghdi [14–16] produced an alternative theory for thermoelastic materials consisting of three models, namely GN I, GN III and GN II, respectively. When these theories are linearized, GN I theory reduces to the classical heat conduction theory and GN III and GN II theories permit thermal signals to propagate with finite speed. GN II theory does not contain the thermal conductivity parameter, and the internal rate of production of entropy is taken to be identically zero, implying no dissipation of thermal energy. GN III includes the previous two theories as special cases and admits dissipation of energy in general. However, these theories do not account for the relaxation time.

In the past few years, it has been seen that an interest is developed to investigate the problems related to initially stressed thermoelastic medium due to its many applications in diverse fields, such as earthquake engineering, geophysics and seismology. Initial stresses are developed in the medium due to many reasons, resulting from the difference of temperature, process of quenching, gravity variations and many more. The problem of an elastic material under initial stress was solved by Biot [17]. For an isotropic medium, Montanaro [18] developed the linear theory of thermoelasticity with hydrostatic initial stress. Effect of rotation in a generalized thermoelastic medium with hydrostatic initial stress under ramp-type loading and heating was studied by Ailawalia and Singh [19]. A two-dimensional problem of an initially stressed fiber-reinforced anisotropic thermoelastic thick plate was considered by Abbas and Abd-Alla [20]. The effect of initial stress on propagation of waves in a fiber-reinforced transversely isotropic medium was investigated in Kumar et al. [21]. The dynamical interactions of diffusion, elastic and thermal fields under initial stress and two temperatures with the fractional-order generalized thermoelasticity were studied by Deswal et al. [22]. Khan and Afzal [23] investigated the effects of gravity, viscosity, initial stress and magnetic field on reflection and refraction of waves at the interface of two viscothermoelastic liquid half-spaces. Deswal et al. [24] analyzed the reflection phenomenon of plane waves at an initially stressed surface of a fiber-reinforced thermoelastic half-space with temperature-dependent properties.

The primary objective of the current work is to investigate the disturbances produced by an inclined load in an

initially stressed fiber-reinforced orthotropic thermoelastic model in the context of GN III theory. Although numerous research problems do exist in a fiber-reinforced transversely isotropic medium, i.e., a thermoelastic medium with fiber reinforcement in one direction only, no attempt has been made to access the distributions of various physical fields, i.e., normal displacement, normal stress, shear stress and temperature distribution in an initially stressed thermoelastic material which is reinforced by fibers in two directions. The exact solutions for displacement, temperature field and stresses are obtained in the physical domain by adopting normal mode analysis. These expressions are computed numerically and illustrated graphically in an orthotropic medium, transversely isotropic medium as well as in isotropic medium. Effects of Green–Naghdi theories (type III and type II), inclination angle of the applied load and time duration are also investigated.

2 Basic equations

The field equations and constitutive relations for an initially stressed fiber-reinforced orthotropic thermoelastic medium with respect to the reinforcement directions \mathbf{a} and \mathbf{b} in the context of combined form of Green–Naghdi theories (type III and type II) are [25]:

$$\begin{aligned} \sigma_{ij} = & -p(\delta_{ij} + w_{ij}) + \lambda e_{kk} \delta_{ij} + 2\mu e_{ij} \\ & + \alpha_1(a_k a_m e_{km} \delta_{ij} + a_i a_j e_{kk}) \\ & + \alpha_2(b_k b_m e_{km} \delta_{ij} + b_i b_j e_{kk}) + 2\mu_1(a_i a_k e_{kj} \\ & + a_j a_k e_{ki}) + 2\mu_2(b_i b_k e_{kj} \\ & + b_j b_k e_{ki}) + \beta_1 a_k a_m e_{km} a_i a_j + \beta_2 b_k b_m e_{km} b_i b_j \\ & + \beta_3(b_k b_m e_{km} a_i a_j \\ & + a_k a_m e_{km} b_i b_j) - \beta_{ij} \theta \delta_{ij}, \end{aligned} \quad (1)$$

$$e_{ij} = \frac{1}{2}(u_{i,j} + u_{j,i}) \quad \text{and} \quad w_{ij} = \frac{1}{2}(u_{j,i} - u_{i,j}), \quad (2)$$

$$\sigma_{ji,j} = \rho \ddot{u}_i, \quad (3)$$

$$K_{ij}^* \theta_{,ij} + \eta K_{ij} \dot{\theta}_{,ij} = \rho c_E \ddot{\theta} + T_0 \beta_{ij} \ddot{u}_{i,j}, \quad (4)$$

where Eq. (1) is the constitutive relation, Eq. (2) is the strain–displacement and rotation–displacement relations, Eq. (3) is the equation of motion with the assumption of absent body forces and Eq. (4) is the heat conduction equation. The parameter $\eta = 1$ makes the heat conduction equation in the context of GN III theory and $\eta = 0$ makes the heat conduction equation in the context of GN II theory, ρ is material density, p is the initially existing stress in the

considered medium, σ_{ij} are stress tensor, e_{ij} are strain tensor, w_{ij} are rotation tensor, u_i are displacement vector, $\alpha_1, \alpha_2, \beta_1, \beta_2, \beta_3, \mu_1$ and μ_2 are reinforcement parameters, λ and μ are Lamé's elastic constants, and δ_{ij} is Kronecker delta. The $\theta = T - T_0$, where T is the absolute temperature and T_0 is the temperature of the material in its natural state assumed to be $|\frac{\theta}{T_0}| \ll 1$. The assumption that the temperature increment is much smaller than T_0 , i.e., $|\frac{\theta}{T_0}| \ll 1$, is essential for a linear theory. Real applications of the present theory such as geological and biological applications satisfy this condition. The material directions are along normalized vectors $\mathbf{a} = (a_1, a_2, a_3)$ and $\mathbf{b} = (b_1, b_2, b_3)$. β_{ij} are thermal elastic coupling tensor, c_E is the specific heat at constant strain, K_{ij} is thermal conductivity such that $K_{ij} = K_i \delta_{ij}$, and K_{ij}^* is material constant such that $K_{ij}^* = K_i^* \delta_{ij}$.

Also, $\beta_{11} = (2\lambda + 3\alpha_1 + 2\mu + \beta_1 + 4\mu_1)\alpha_{1t} + (\lambda + \alpha_1 + \alpha_2 + \beta_3)\alpha_{2t}$,
 $\beta_{22} = (2\lambda + \alpha_1 + 2\alpha_2 + \beta_3)\alpha_{1t} + (\lambda + 2\mu + 2\alpha_2 + \beta_2 + 4\mu_2)\alpha_{2t}$,

where α_{1t} and α_{2t} are coefficients of linear thermal expansion.

In the above considered equations, a dot denotes partial temporal derivative and comma indicates spatial derivative.

3 Problem formulation

A semi-infinite orthotropic medium in a two-dimensional space ($x \geq 0, -\infty \leq y \leq \infty$) is considered as shown in Fig. 1. The considered medium is initially stressed.

The displacement components in plane problem are $u = u_1 = u(x, y, t)$ and $v = u_2 = v(x, y, t)$ where $w = u_3 = 0$.

The fiber directions are along the x - and y - directions such that $\mathbf{a} = (1, 0, 0)$ and $\mathbf{b} = (0, 1, 0)$. The stress components ($\sigma_{ij}, i, j = 1, 2$) are reduced according to Eq. (1) to the following

$$\sigma_{xx} = -p + H_{11} \frac{\partial u}{\partial x} + H_{12} \frac{\partial v}{\partial y} - \beta_{11} \theta, \tag{5}$$

$$\sigma_{yy} = -p + H_{12} \frac{\partial u}{\partial x} + H_{13} \frac{\partial v}{\partial y} - \beta_{22} \theta, \tag{6}$$

$$\sigma_{xy} = H_{17} \frac{\partial u}{\partial y} + H_{15} \frac{\partial v}{\partial x}, \tag{7}$$

$$\sigma_{yx} = H_{15} \frac{\partial u}{\partial y} + H_{17} \frac{\partial v}{\partial x}, \tag{8}$$

where

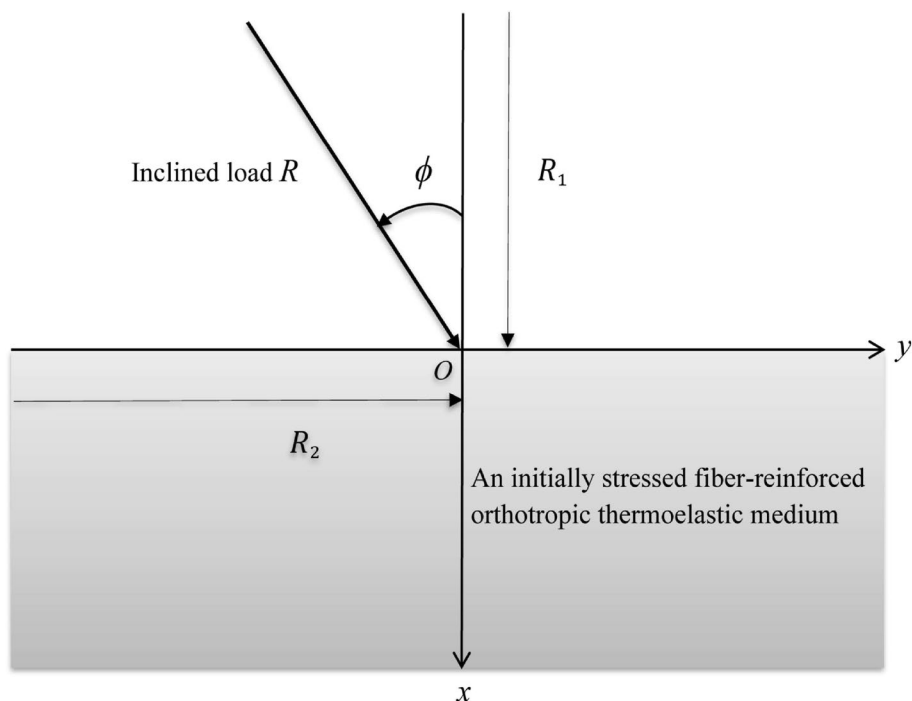
$$H_{11} = \lambda + 2\mu + 2\alpha_1 + \beta_1 + 4\mu_1, \quad H_{12} = \lambda + \alpha_1 + \alpha_2 + \beta_3,$$

$$H_{13} = \lambda + 2\mu + 2\alpha_2 + \beta_2 + 4\mu_2, \quad H_{14} = \mu + \mu_1 + \mu_2,$$

$$H_{15} = -\frac{p}{2} + H_{14}, \quad H_{17} = \frac{p}{2} + H_{14}.$$

Upon substituting the stresses in Eq. (5) through (8), into the equation of motion (3) with the assumption of plane problem, one can obtain the following

Fig. 1 Semi-infinite plane subjected to an inclined load



$$\rho \frac{\partial^2 u}{\partial t^2} = H_{11} \frac{\partial^2 u}{\partial x^2} + H_{15} \frac{\partial^2 u}{\partial y^2} + H_{16} \frac{\partial^2 v}{\partial x \partial y} - \beta_{11} \frac{\partial \theta}{\partial x}, \tag{9}$$

$$\rho \frac{\partial^2 v}{\partial t^2} = H_{13} \frac{\partial^2 v}{\partial y^2} + H_{15} \frac{\partial^2 v}{\partial x^2} + H_{16} \frac{\partial^2 u}{\partial x \partial y} - \beta_{22} \frac{\partial \theta}{\partial y}, \tag{10}$$

where

$$H_{16} = H_{12} + H_{14} + \frac{p}{2}.$$

The heat conduction equation (4) is therefore reduced to

$$\begin{aligned} K_1^* \frac{\partial^2 \theta}{\partial x^2} + K_2^* \frac{\partial^2 \theta}{\partial y^2} + \eta \frac{\partial}{\partial t} \left(K_1 \frac{\partial^2 \theta}{\partial x^2} + K_2 \frac{\partial^2 \theta}{\partial y^2} \right) \\ = \rho c_E \ddot{\theta} + T_0 \beta_{11} \frac{\partial \ddot{u}}{\partial x} \\ + T_0 \beta_{22} \frac{\partial \ddot{v}}{\partial y}. \end{aligned} \tag{11}$$

The following dimensionless quantities are introduced to transform Eqs. (5)–(11) into a nondimensional form

$$\begin{aligned} (x', y', u', v') &= c_0 \eta_0 (x, y, u, v), \\ t' &= c_0^2 \eta_0 t, \quad \theta' = \frac{\beta_{11}}{\rho c_0^2} \theta, \\ (\sigma'_{ij}, p') &= \frac{1}{\rho c_0^2} (\sigma_{ij}, p), \quad i, j = 1, 2 \end{aligned} \tag{12}$$

where

$$\eta_0 = \frac{\rho c_E}{K_1}, \quad c_0^2 = \frac{H_{11}}{\rho}.$$

Using the nondimensional form, Eq. (5) through (11) can be written as

$$\sigma_{xx} = -p + \frac{\partial u}{\partial x} + I_1 \frac{\partial v}{\partial y} - \theta, \tag{13}$$

$$\sigma_{xy} = I_7 \frac{\partial u}{\partial y} + I_5 \frac{\partial v}{\partial x}, \tag{14}$$

$$\sigma_{yx} = I_5 \frac{\partial u}{\partial y} + I_7 \frac{\partial v}{\partial x}, \tag{15}$$

$$\sigma_{yy} = -p + I_1 \frac{\partial u}{\partial x} + I_2 \frac{\partial v}{\partial y} - I_3 \theta, \tag{16}$$

$$\frac{\partial^2 u}{\partial t^2} = \frac{\partial^2 u}{\partial x^2} + I_6 \frac{\partial^2 v}{\partial x \partial y} + I_5 \frac{\partial^2 u}{\partial y^2} - \frac{\partial \theta}{\partial x}, \tag{17}$$

$$\frac{\partial^2 v}{\partial t^2} = I_5 \frac{\partial^2 v}{\partial x^2} + I_6 \frac{\partial^2 u}{\partial x \partial y} + I_2 \frac{\partial^2 v}{\partial y^2} - I_3 \frac{\partial \theta}{\partial y}, \tag{18}$$

$$\begin{aligned} I_9 \frac{\partial^2 \theta}{\partial x^2} + I_{10} \frac{\partial^2 \theta}{\partial y^2} + \eta \frac{\partial}{\partial t} \left(\frac{\partial^2 \theta}{\partial x^2} + I_{11} \frac{\partial^2 \theta}{\partial y^2} \right) \\ = \frac{\partial^2 \theta}{\partial t^2} + I_{12} \frac{\partial \ddot{u}}{\partial x} + I_8 \frac{\partial \ddot{v}}{\partial y}, \end{aligned} \tag{19}$$

where

$$\begin{aligned} (I_1, I_2, I_4) &= \frac{1}{H_{11}} (H_{12}, H_{13}, H_{14}), I_3 = \frac{\beta_{22}}{\beta_{11}}, I_5 = I_4 - \frac{p}{2}, \\ I_6 &= I_1 + I_4 + \frac{p}{2}, I_7 = I_4 + \frac{p}{2}, I_8 = \frac{T_0 \beta_{11} \beta_{22}}{K_1 H_{11} \eta_0}, \\ I_9 &= \frac{K_1^*}{c_0^2 \eta_0 K_1}, I_{10} = \frac{K_2^*}{c_0^2 \eta_0 K_1}, I_{11} = \frac{K_2}{K_1}, I_{12} = \frac{T_0 \beta_{11}^2}{K_1 H_{11} \eta_0}. \end{aligned}$$

4 Normal mode analysis

In the current section, normal mode technique is applied to obtain the exact solutions without any presumed constraints on the physical fields. It was applied to a wide range of problems for different cases (Othman and Lotfy [8], Ezzat and Awad [26]). The physical fields under consideration and the components of stress are transformed in terms of normal modes, using

$$\begin{aligned} [u, v, \theta, \sigma_{ij}, p](x, y, t) \\ = [u^*, v^*, \theta^*, \sigma_{ij}^*, p^*](x) \exp(\omega t + imy), \end{aligned} \tag{20}$$

where ω is the frequency (a complex constant), m is the wave number in y -direction, i is the imaginary unit and $u^*, v^*, \theta^*, \sigma_{ij}^*$ and p^* are the magnitudes of the functions $u, v, \theta, \sigma_{ij}$ and p , respectively.

From Eq. (20), Eqs. (17)–(19) can be written in the following form:

$$(D^2 - J_1)u^* + J_2 Dv^* - D\theta^* = 0, \tag{21}$$

$$J_2 Du^* + (I_5 D^2 - J_3)v^* - J_4 \theta^* = 0, \tag{22}$$

$$J_5 Du^* + J_6 v^* - (J_7 D^2 - J_8)\theta^* = 0, \tag{23}$$

where

$$\begin{aligned} D &= \frac{d}{dx}, \quad J_1 = I_5 m^2 + \omega^2, \\ J_2 &= imI_6, \quad J_3 = I_2 m^2 + \omega^2, \\ J_4 &= imI_3, \quad J_5 = I_{12} \omega^2, \\ J_6 &= imI_8 \omega^2, \quad J_7 = I_9 + \eta \omega, \\ J_8 &= m^2 (I_{10} + \eta \omega I_{11}) + \omega^2. \end{aligned}$$

Equations (21)–(23) represent a system of linear differential equations in terms of the physical variables u^* , v^* and θ^* . Upon simplifying the previous equations, one can get the following sixth-order differential equation

$$[D^6 - QD^4 + SD^2 - T][u^*, v^*, \theta^*] = 0, \tag{24}$$

where

$$Q = \frac{A_1A_7 + A_2A_6 + I_5A_5 + A_3A_4}{A_1A_6 + I_5A_4},$$

$$S = \frac{A_1A_8 + A_2A_7 + A_3A_5}{A_1A_6 + I_5A_4},$$

$$T = \frac{A_2A_8}{A_1A_6 + I_5A_4},$$

$$A_1 = J_4 - J_2, \quad A_2 = J_4J_1,$$

$$A_3 = J_4J_2 + J_3, \quad A_4 = J_2J_7,$$

$$A_5 = J_2J_8 + J_4J_5, \quad A_6 = J_7I_5,$$

$$A_7 = J_7J_3 + J_8I_5, \quad A_8 = J_8J_3 - J_4J_6.$$

The above equation can be factorized as

$$[(D^2 - \lambda_1^2)(D^2 - \lambda_2^2)(D^2 - \lambda_3^2)][u^*(x), v^*(x), \theta^*(x)] = 0, \tag{25}$$

where λ_n^2 , ($n = 1, 2, 3$) are the zeros of the following characteristic equation

$$\lambda^6 - Q\lambda^4 + S\lambda^2 - T = 0. \tag{26}$$

The solution of Eq. (24), which is bounded as $x \rightarrow \infty$, has the following form

$$(u^*, v^*, \theta^*) = \sum_{n=1}^3 (H_n, H'_n, H''_n)(m, \omega) e^{-\lambda_n x}, \tag{27}$$

where H_n, H'_n and H''_n are parameters that depend on ω and m and the parameters H_n are determined from imposing boundary conditions. Substitution of Eq. (27) in the system of Eqs. (21)–(23) yields

$$(v^*, \theta^*) = \sum_{n=1}^3 (N_{1n}, N_{2n}) H_n(m, \omega) e^{-\lambda_n x}, \tag{28}$$

where

$$N_{1n} = \frac{(A_1\lambda_n^2 - A_2)}{\lambda_n(I_5\lambda_n^2 - A_3)} \quad \text{and} \quad N_{2n} = \frac{\lambda_n^2 + J_2N_{1n}\lambda_n - J_1}{\lambda_n}.$$

With the aid of nondimensional quantities defined in (12) and normal mode analysis, the expressions of stresses (13)–(16) take the forms

$$\sigma_{xx}^* = -p^* + \sum_{n=1}^3 N_{3n} H_n(m, \omega) e^{-\lambda_n x}, \tag{29}$$

$$\sigma_{xy}^* = \sum_{n=1}^3 N_{4n} H_n(m, \omega) e^{-\lambda_n x}, \tag{30}$$

$$\sigma_{yx}^* = \sum_{n=1}^3 N_{5n} H_n(m, \omega) e^{-\lambda_n x}, \tag{31}$$

$$\sigma_{yy}^* = -p^* + \sum_{n=1}^3 N_{6n} H_n(m, \omega) e^{-\lambda_n x}, \tag{32}$$

where

$$N_{3n} = -\lambda_n + \text{im}I_1N_{1n} - N_{2n}, \quad N_{4n} = I_7\text{im} - I_5\lambda_nN_{1n},$$

$$N_{5n} = I_5\text{im} - I_7\lambda_nN_{1n}, \quad N_{6n} = -I_1\lambda_n + \text{im}I_2N_{1n} - I_3N_{2n}.$$

5 Application

A fiber-reinforced orthotropic thermoelastic medium with an initially presented stress p , occupying the half-space ($x \geq 0, -\infty \leq y \leq \infty$), as shown in Fig. 1 is considered. The surface of the half-space, i.e., the plane $x = 0$, is subjected to an inclined load $\mathbf{R}(R_1, R_2, 0)$ with an inclination angle ϕ , defined from the negative x -axis as shown in Fig. 1. The applied load R is decomposed as a normal load $R_1 = R \cos \phi$ and shear load $R_2 = R \sin \phi$. The surface of the medium is kept at reference temperature T_0 ; hence, the boundary conditions can be written as

$$\theta(0, y, t) = 0, \tag{33}$$

$$\sigma_{xx}(0, y, t) = -p - R_1, \tag{34}$$

$$\sigma_{xy}(0, y, t) = -R_2. \tag{35}$$

With the help of normal mode technique, the boundary conditions in terms of the stresses defined in (29) and (30) are written as

$$\theta^* = 0, \tag{36}$$

$$\sigma_{xx}^* = -p^* - R_1^*, \tag{37}$$

$$\sigma_{xy}^* = -R_2^* \quad \text{at } x = 0. \tag{38}$$

where $R_1^* = R^* \cos \phi$, $R_2^* = R^* \sin \phi$ and R^* is defined by the expression

$$R = R^* \exp(\omega t + imy).$$

Using expressions (28)–(30), the boundary conditions (36)–(38) yield a nonhomogeneous system of three equations, which can be expressed in matrix form as

$$\begin{bmatrix} N_{21} & N_{22} & N_{23} \\ N_{31} & N_{32} & N_{33} \\ N_{41} & N_{42} & N_{43} \end{bmatrix} \begin{bmatrix} H_1 \\ H_2 \\ H_3 \end{bmatrix} = \begin{bmatrix} 0 \\ -R_1^* \\ -R_2^* \end{bmatrix}. \tag{39}$$

The expressions for H_n , ($n = 1, 2, 3$) procured by solving the system (39) are given as

$$H_1 = \frac{\Delta_1}{\Delta}, \quad H_2 = \frac{\Delta_2}{\Delta}, \quad H_3 = \frac{\Delta_3}{\Delta}, \tag{40}$$

where

$$\begin{aligned} \Delta_1 &= -N_{22}(-R_1^*N_{43} + R_2^*N_{33}) + N_{23}(-R_1^*N_{42} + R_2^*N_{32}), \\ \Delta_2 &= N_{21}(-R_1^*N_{43} + R_2^*N_{33}) + N_{23}(-R_2^*N_{31} + R_1^*N_{41}), \\ \Delta_3 &= N_{21}(-R_2^*N_{32} + R_1^*N_{42}) - N_{22}(-R_2^*N_{31} + R_1^*N_{41}), \\ \Delta &= N_{21}(N_{32}N_{43} - N_{42}N_{33}) - N_{22}(N_{31}N_{43} - N_{41}N_{33}) \\ &\quad + N_{23}(N_{31}N_{42} - N_{32}N_{41}). \end{aligned}$$

Substitution of Eq. (40) in Eqs. (27)–(32) gives the following expressions of displacement, temperature and stress components

$$u(x, y, t) = \frac{1}{\Delta} [\Delta_1 e^{-\lambda_1 x} + \Delta_2 e^{-\lambda_2 x} + \Delta_3 e^{-\lambda_3 x}] e^{\omega t + imy}, \tag{41}$$

$$v(x, y, t) = \frac{1}{\Delta} [N_{11} \Delta_1 e^{-\lambda_1 x} + N_{12} \Delta_2 e^{-\lambda_2 x} + N_{13} \Delta_3 e^{-\lambda_3 x}] e^{\omega t + imy}, \tag{42}$$

$$\theta(x, y, t) = \frac{1}{\Delta} [N_{21} \Delta_1 e^{-\lambda_1 x} + N_{22} \Delta_2 e^{-\lambda_2 x} + N_{23} \Delta_3 e^{-\lambda_3 x}] e^{\omega t + imy}, \tag{43}$$

$$\sigma_{xx}(x, y, t) = -p + \frac{1}{\Delta} [N_{31} \Delta_1 e^{-\lambda_1 x} + N_{32} \Delta_2 e^{-\lambda_2 x} + N_{33} \Delta_3 e^{-\lambda_3 x}] e^{\omega t + imy}, \tag{44}$$

$$\sigma_{xy}(x, y, t) = \frac{1}{\Delta} [N_{41} \Delta_1 e^{-\lambda_1 x} + N_{42} \Delta_2 e^{-\lambda_2 x} + N_{43} \Delta_3 e^{-\lambda_3 x}] e^{\omega t + imy}, \tag{45}$$

$$\sigma_{yx}(x, y, t) = \frac{1}{\Delta} [N_{51} \Delta_1 e^{-\lambda_1 x} + N_{52} \Delta_2 e^{-\lambda_2 x} + N_{53} \Delta_3 e^{-\lambda_3 x}] e^{\omega t + imy}, \tag{46}$$

$$\begin{aligned} \sigma_{yy}(x, y, t) &= -p + \frac{1}{\Delta} [N_{61} \Delta_1 e^{-\lambda_1 x} + N_{62} \Delta_2 e^{-\lambda_2 x} \\ &\quad + N_{63} \Delta_3 e^{-\lambda_3 x}] e^{\omega t + imy}. \end{aligned} \tag{47}$$

6 Particular cases

To validate the theoretical/numerical results of the current investigation, different particular cases are considered as listed in Table 1.

6.1 Transversely isotropic medium

To discuss the problem in an initially stressed fiber-reinforced transversely isotropic thermoelastic half-space in the context of GN III theory (i.e., with parameter $\eta = 1$), it is sufficient to set the values of fiber reinforcement parameters as: $\alpha_1 = \alpha, \beta_1 = \beta, \mu = \mu_T, \mu_1 = \mu_L - \mu_T, \mu_2 = \alpha_2 = \beta_2 = \beta_3 = 0$. In this case, the material is reinforced with the fibers in a single direction only, which are randomly distributed in the cross sections normal to the fibers. Then, the composite material has a single preferred direction (fiber direction) and so is transversely isotropic with respect to this direction and only five stiffness coefficients will remain in the constitutive relation, to characterize the thermoelastic response of transversely isotropic material. Along with these modifications and setting the parameters $\phi = 0^\circ, p = 0$ and $\eta = 1$, the results obtained in this case match with those of Abbas [2], by applying thermal load instead of mechanical load in the boundary condition.

6.2 Isotropic medium

By setting the parameters as: $\alpha_1 = \alpha, \beta_1 = \beta, \mu = \mu_T, \mu_1 = \mu_L - \mu_T, \mu_2 = \alpha_2 = \beta_2 = \beta_3 = 0$, along with $\phi = 0^\circ, p = 0$ and $\eta = 1$, in Eqs. (1)–(4) of this paper, the basic governing equations for a transversely isotropic medium are obtained as follows

$$\begin{aligned} \sigma_{ij} &= \lambda e_{kk} \delta_{ij} + 2\mu_T e_{ij} + \alpha(a_k a_m e_{km} \delta_{ij} + a_i a_j e_{kk}) \\ &\quad + \beta a_k a_m e_{km} a_i a_j + 2(\mu_L - \mu_T)(a_i a_k e_{kj} + a_j a_k e_{ki}) - \beta_{ij} \theta \delta_{ij}, \end{aligned} \tag{48}$$

$$e_{ij} = \frac{1}{2}(u_{i,j} + u_{j,i}), \tag{49}$$

$$\sigma_{ji,j} = \rho \ddot{u}_i, \tag{50}$$

Table 1 Tabular representation of particular cases of the considered model

Model	Specifications of the model	
Orthotropic medium	An initially stressed thermoelastic medium with fiber reinforcement in two directions in the context of GN-III theory	
<i>Particular cases</i>		
1	Transversely isotropic medium	An initially stressed thermoelastic medium with fiber reinforcement in one direction in the context of GN-III theory
2	Isotropic medium	An initially stressed thermoelastic medium without fiber reinforcement in the context of GN-III theory
3	Absence of initial stress	A thermoelastic medium with fiber reinforcement in two directions in the context of GN-III theory
4	Green–Naghdi theory of type II	An initially stressed thermoelastic medium with fiber reinforcement in two directions in the context of GN-II theory

$$K_{ij}^* \theta_{,ij} + K_{ij} \dot{\theta}_{,ij} = \rho c_E \ddot{\theta} + T_0 \beta_{ij} \ddot{u}_{i,j}, \quad (51)$$

which are exactly same as Eqs. (2)–(5) in Othman and Atwa [27]. Also Eq. (1) of Othman and Atwa [27] implies that the geometry of both the cases is exactly same, and correspondingly, the results derived in this case are exactly same as obtained in equations (50)–(56) of Othman and Atwa [27]. Further setting parameters as: $\alpha = \beta = 0$, $\mu_L = \mu_T$, $K_1 = K_2$, $K_1^* = K_2^*$, $\beta_{11} = \beta_{22} = (3\lambda + 2\mu)\alpha_t$, $\alpha_{1t} = \alpha_{2t} = \alpha_t$ in formulation of transversely isotropic case of this paper and Othman and Atwa [27], one can get the exactly same results for an isotropic thermoelastic medium in the context of GN III model.

This fully matching of the problem formulation and the results derived in particular case of this paper and Othman and Atwa [27] gives a proper validation to the results obtained.

6.3 Absence of initial stress

The relevant expressions of field variables in this particular case can be obtained in an orthotropic thermoelastic medium in the context of GN III theory if the value of initial stress p is set equal to zero in constitutive relations.

6.4 Green–Naghdi theory type II (GN II)

By setting the parameter η zero, the expressions of physical fields can be obtained from the expressions (41)–(47).

7 Numerical results and discussion

With a view to demonstrate the analytical expressions presented earlier, some numerical results which depict the interpretations of normal displacement field, normal stress field, shear stress field and temperature distribution field are

presented. The numerical computation is performed with the help of MATLAB software. For this purpose, the values of some relevant physical constants are taken from Abbas et al. [28] for a magnesium crystal-like material and these material constants are listed in Table 2.

The solution expressed by relation (20) consists of the term $e^{(\omega t + i m y)}$, where ω is the frequency (a complex constant) and can be expanded as $\omega = \omega_1 + i\omega_2$. The expression $e^{\omega t} = e^{\omega_1 t} e^{i\omega_2 t}$ is approximately equal to $e^{\omega_1 t}$ for small values of time because $e^{i\omega_2 t} = \cos \omega_2 t + i \sin \omega_2 t \rightarrow 1$ as $t \rightarrow 0$. Therefore, one can consider ω as real (i.e., $\omega = \omega_1$). The values of parameters for numerical calculation are considered as: $\omega = 1.0$, $m = 1.1$, $\eta = 1$, $R^* = 1.0$, $\phi = 30^\circ$ and $p = 0.05$. Using the above numerical values of the parameters, values of the nondimensional field variables have been evaluated and results are plotted at different locations of x at $t = 0.01$ s and $y = 1$.

For convenience, we have classified the figures into four different groups: The first group (Figs. 2, 3, 4, 5) examines the influence of the fiber reinforcement on various field variables. In the second group (Figs. 6, 7, 8, 9), all the physical fields have been examined for fiber-reinforced thermoelastic model in the context of GN III and in the presence of initial stress (solid line), in context with GN III and in the absence of initial stress (dashed line), in the context of GN II and in the presence of initial stress (dotted line) and in context with GN II and in the absence of initial stress (dash-dotted line). The third group (Figs. 10, 11, 12, 13) is concerned with the two-dimensional plots of various physical fields to analyze the effect of inclination of load for the assumed model by considering four distinct values of angle as $\phi = 0^\circ$ (solid line), $\phi = 30^\circ$ (dashed line), $\phi = 60^\circ$ (dotted line) and $\phi = 90^\circ$ (dash-dotted line). In the last group (Figs. 14, 15, 16, 17), the variations in physical fields are depicted to examine the effects of time t on them for three distinct instants (0.01, 0.05 and 0.10).

Table 2 Numerical values of material parameters

Parameter	Units	Values	Parameter	Units	Values
ρ	kg m^{-3}	2660	λ	$\text{kg m}^{-1} \text{s}^{-2}$	5.65×10^{10}
μ	$\text{kg m}^{-1} \text{s}^{-2}$	2.46×10^{10}	μ_1	$\text{kg m}^{-1} \text{s}^{-2}$	3.2×10^{10}
μ_2	$\text{kg m}^{-1} \text{s}^{-2}$	3.3×10^{10}	T_0	K	293
α_1	$\text{kg m}^{-1} \text{s}^{-2}$	-1.28×10^{10}	α_2	$\text{kg m}^{-1} \text{s}^{-2}$	-1.27×10^{10}
β_1	$\text{kg m}^{-1} \text{s}^{-2}$	220.9×10^{10}	β_2	$\text{kg m}^{-1} \text{s}^{-2}$	224.1×10^{10}
β_3	$\text{kg m}^{-1} \text{s}^{-2}$	227.3×10^{10}	c_E	$\text{J kg}^{-1} \text{deg}^{-1}$	0.787×10^3
α_{1t}	deg^{-1}	0.017×10^{-4}	α_{12}	deg^{-1}	0.015×10^{-4}
K_1	$\text{J m}^{-1} \text{s}^{-1} \text{deg}^{-1}$	0.0921×10^3	K_2	$\text{J m}^{-1} \text{s}^{-1} \text{deg}^{-1}$	0.0963×10^3
K_1^*	$\text{J m}^{-1} \text{s}^{-2} \text{deg}^{-1}$	1.313×10^2	K_2^*	$\text{J m}^{-1} \text{s}^{-2} \text{deg}^{-1}$	1.540×10^2

Fig. 2 Variation in normal displacement for different fiber reinforcements at $y = 1$

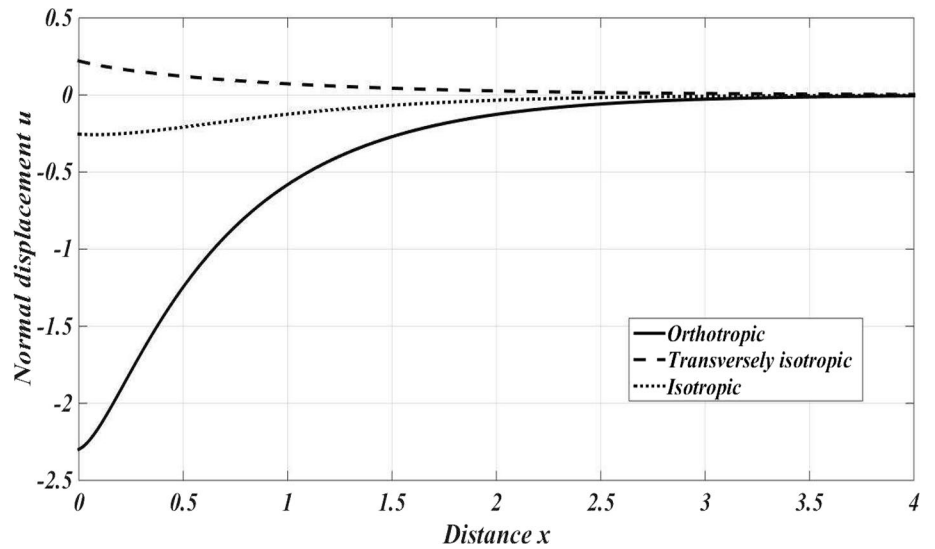


Fig. 3 Variation in normal stress for different fiber reinforcements at $y = 1$

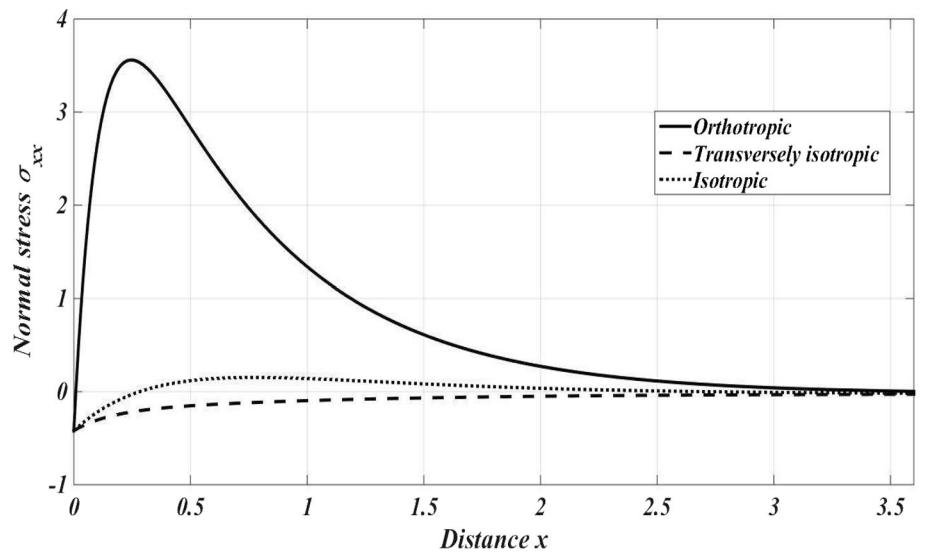


Fig. 4 Variation in shear stress for different fiber reinforcements at $y = 1$

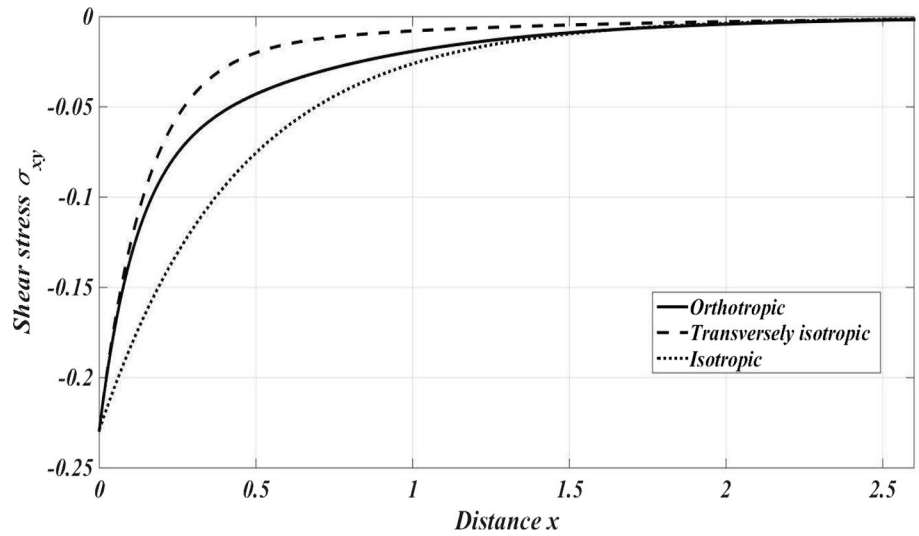


Fig. 5 Variation in temperature field for different fiber reinforcements at $y = 1$

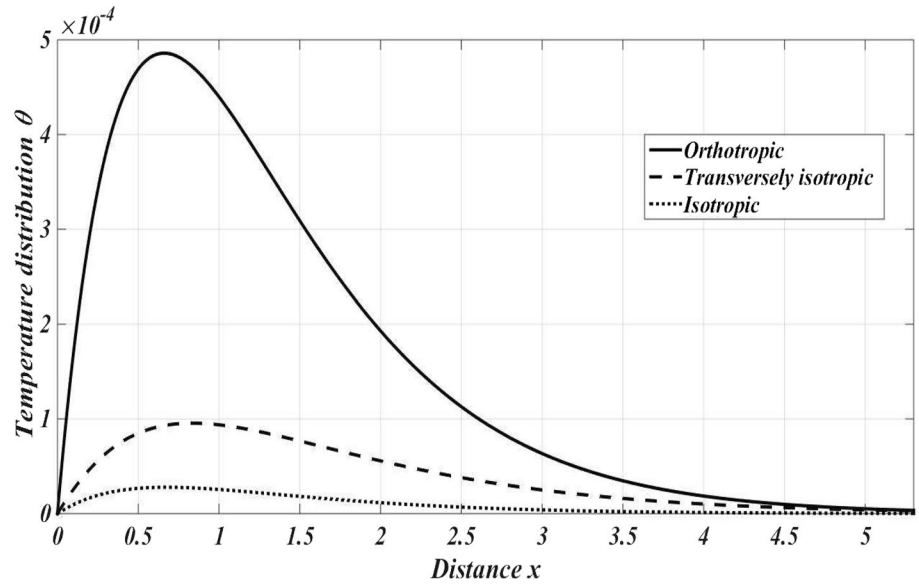


Fig. 6 Effect of initial stress and Green–Naghdi theories (type III and type II) on normal displacement at $y = 1$

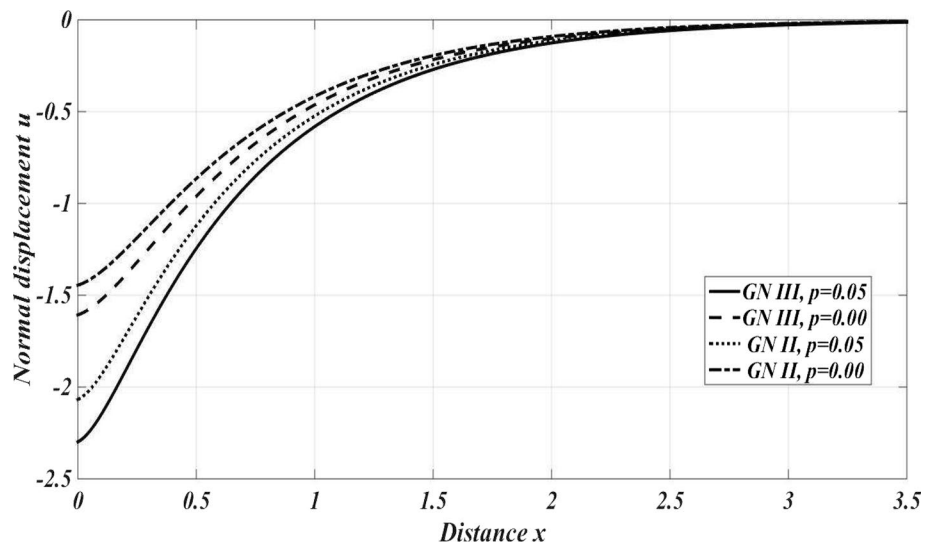


Fig. 7 Effect of initial stress and Green–Naghdi theories (type III and type II) on normal stress at $y = 1$

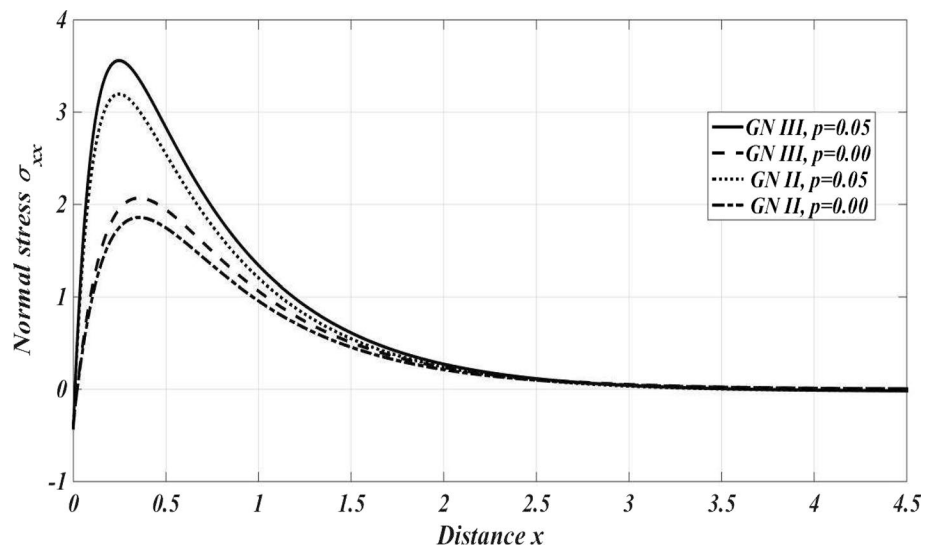


Fig. 8 Effect of initial stress and Green–Naghdi theories (type III and type II) on shear stress at $y = 1$

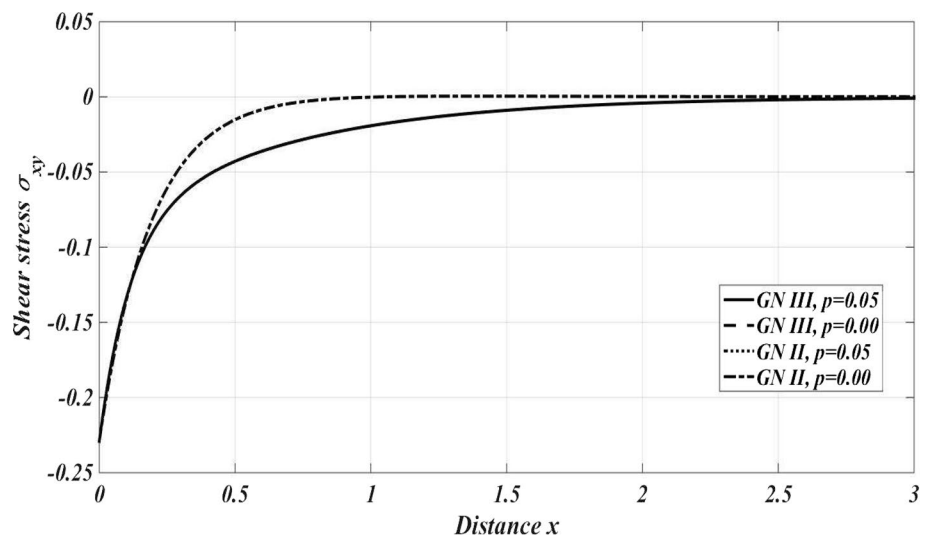
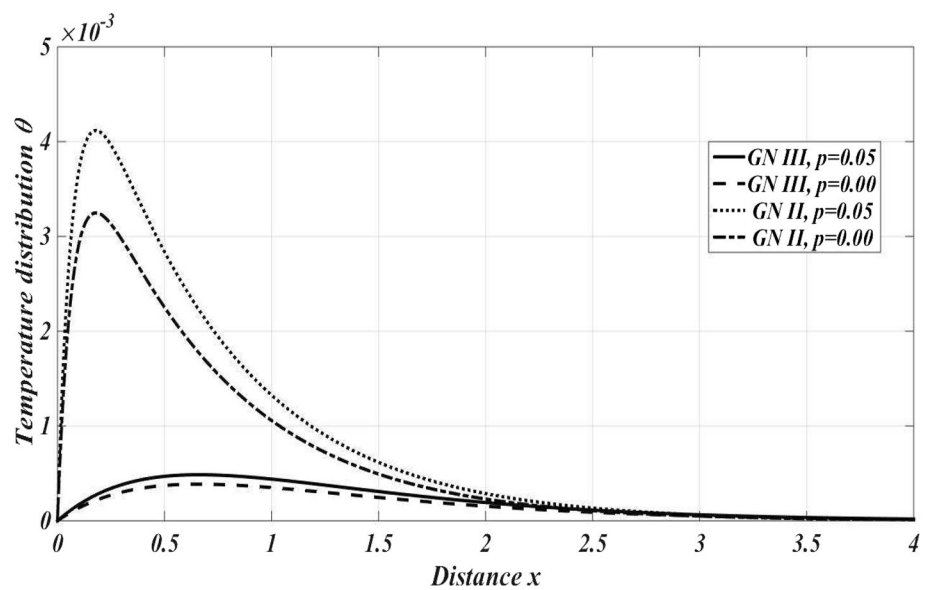


Fig. 9 Effect of initial stress and Green–Naghdi theories (type III and type II) on temperature field at $y = 1$



7.1 Effect of fiber reinforcement

Figure 2 depicts the spatial variations in the normal displacement u with distance x for the three different media (orthotropic medium, transversely isotropic medium and isotropic). Solution curves for all the cases start with different starting values, which shows the significant influence of fiber reinforcement. Figure 3 displays the variations in normal stress with distance x . In this figure, all the solution curves have coincident beginning point with value -0.4468 and coincident ending point with value -0.0500 , which satisfies the boundary conditions, since the initial stress is present already in the medium. It reveals the compressive nature of normal stress in the transversely isotropic and isotropic media while the curve corresponding to orthotropic medium spreads more than the others.

Figure 4 clarifies the variations in the shear stress σ_{xy} corresponding to the three cases: orthotropic, transversely isotropic and isotropic media against the distance x . The figure exhibits that shear stress is compressive for the whole range of distance x . Variations in temperature θ with space coordinate x are displayed in Fig. 5. It is noticed that the temperature distribution has a coincident starting point of zero magnitude, which is in well accordance with the boundary condition. Also, the values of this field are maximum for the orthotropic fiber-reinforced medium and are higher for the transversely isotropic fiber-reinforced medium than those for an isotropic medium. The figure shows that the presence of fiber reinforcement increases the magnitude of temperature in the entire range.

Fig. 10 Effect of inclination angle of load on normal displacement at $y = 1$

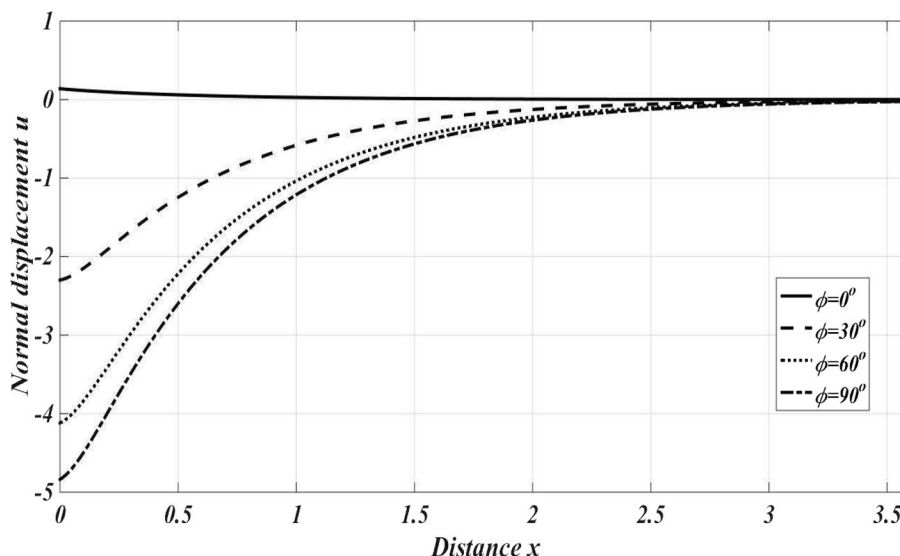


Fig. 11 Effect of inclination angle of load on normal stress at $y = 1$

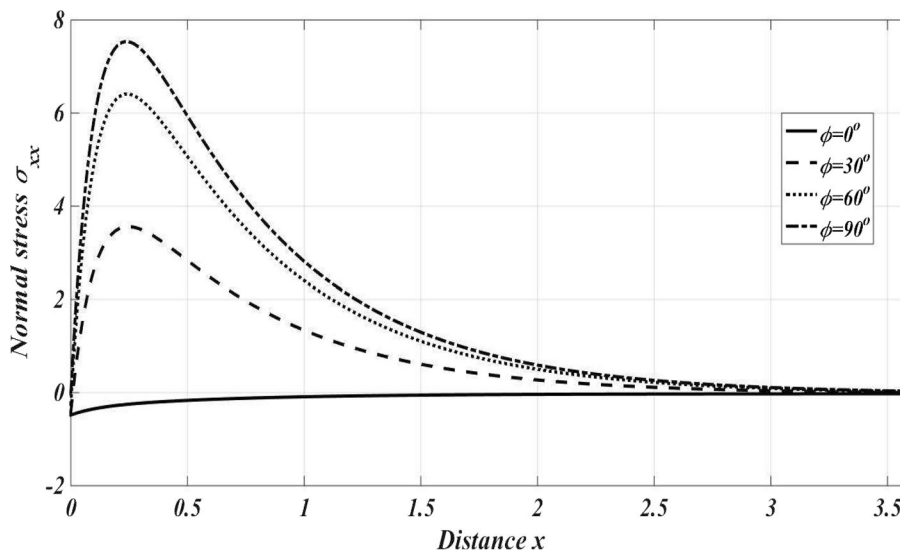


Fig. 12 Effect of inclination angle of load on shear stress at $y = 1$

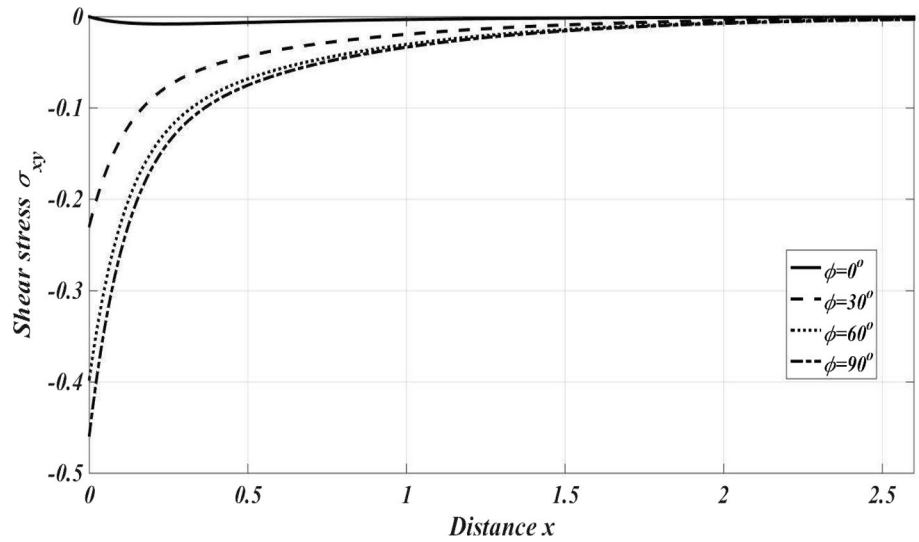


Fig. 13 Effect of inclination angle of load on temperature field at $y = 1$

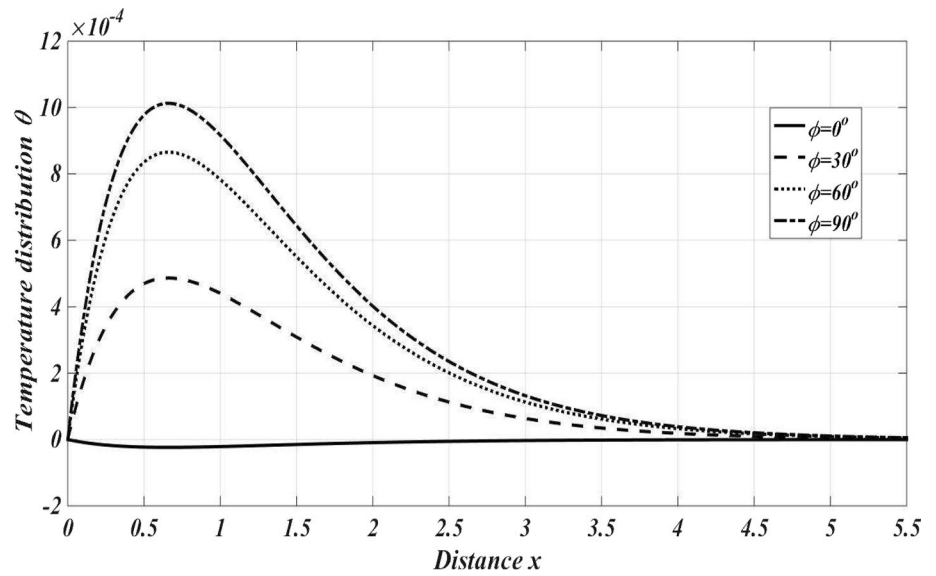


Fig. 14 Effect of time on normal displacement at $y = 1$

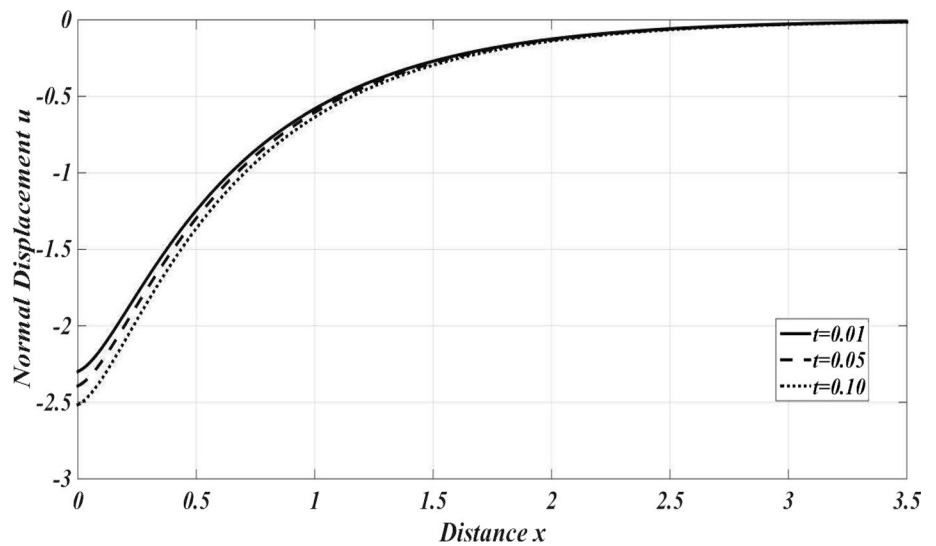


Fig. 15 Effect of time on normal stress at $y = 1$

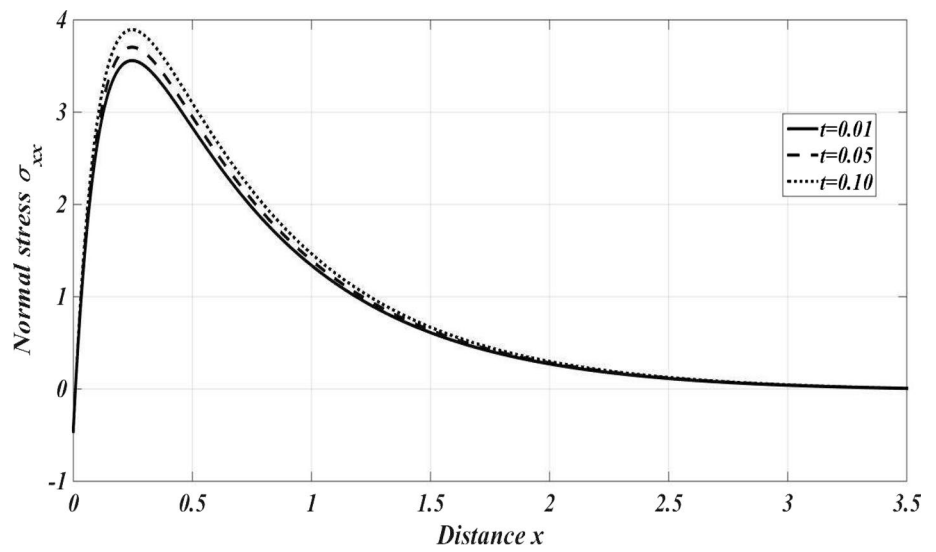


Fig. 16 Effect of time on shear stress at $y = 1$

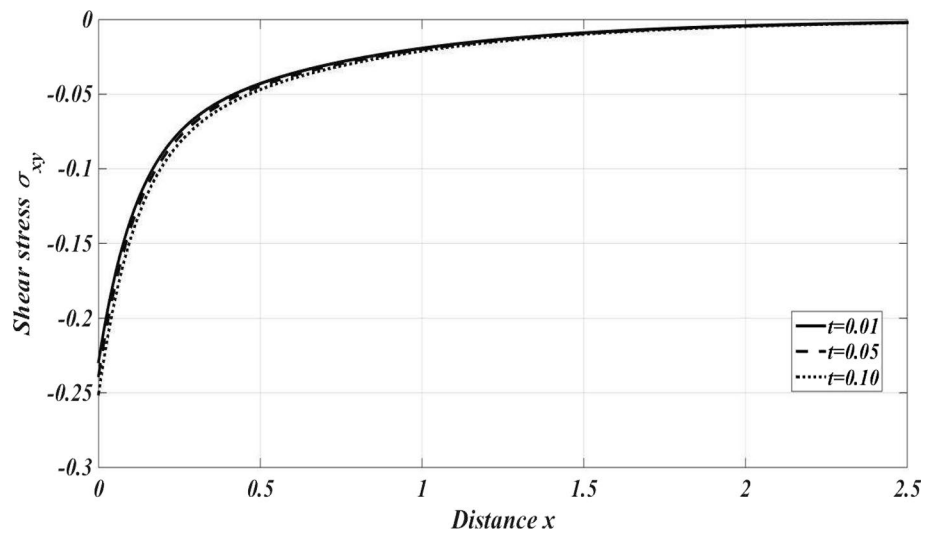
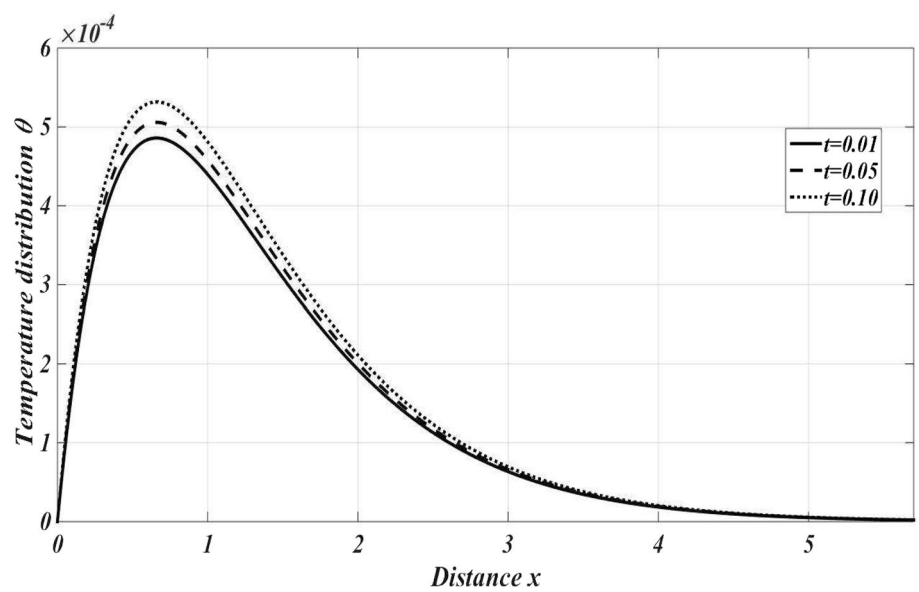


Fig. 17 Effect of time on temperature field at $y = 1$



7.2 Effect of initial stress and Green–Naghdi theories

Figure 6 shows the variations in normal displacement u against the location x for the four cases: GN III theory in the presence of initial stress, GN III theory in the absence of initial stress, GN II theory in the presence of initial stress and GN II theory in the absence of initial stress. The presence of initial stress increases the magnitude of normal displacement for both the theories. Figure 7 reveals the variations in normal stress in the context of all the above-mentioned four cases. A careful view of the figure emphasizes on the point that for a fixed value of initial stress, the magnitude of normal stress in the context of GN III theory is higher as compared to the normal stress in the context of GN II theory in the region $0.01 \leq x \leq 3.10$, and the normal stress shows reverse behavior in the rest of domain. As expected, for both the theories, the solution curves follow similar pattern of variations with difference in magnitudes.

The distribution of shear stress against the distance x , depicted in Fig. 8, attains a similar pattern for all the four models. The plot shows that the curves for GN II theory and GN III theory overlap, which indicates that GN theories exhibit same profile of shear stress. The pattern of distribution of temperature field with the location x is depicted in Fig. 9. Temperature field begins from the coincident starting value zero and gets the maximum impact as x approaches 0.15, and this impact diminishes completely as $x \geq 4.0$. Also, the curves attain higher values for GN II theory as compared to GN III theory and the initial stress causes an increase in the value of temperature distribution.

7.3 Effect of inclination angle

In Fig. 10, a similar trend of distribution of normal displacement is depicted for three distinct values of inclination angle ϕ (i.e., $\phi = 30^\circ, 60^\circ$ and 90°), whereas for $\phi = 0^\circ$, it exhibits reverse behavior. The figure reveals that the value of normal displacement corresponding to angle $\phi = 0^\circ$ is positive while that corresponding to other values of angle ϕ is negative. Also, an increase in the value of ϕ results in an increase in the magnitude of displacement field. Figure 11 exhibits the distribution of normal stress against distance x for four different values of ϕ . The behavior of normal stress for $\phi = 30^\circ, 60^\circ$ and 90° is almost similar with difference in magnitudes while the curve corresponding to $\phi = 0^\circ$ shows different behaviors. Inclination angle of load has significant increasing effect on the normal stress in the region $0.01 \leq x \leq 3.16$ and has different effects in rest of the domain.

Figure 12 represents the compressive nature of the shear stress σ_{xy} against the distance x . The figure shows that corresponding to $\phi = 30^\circ, 60^\circ$ and 90° , the shear stress starts

with negative numerical values and then tends to zero as x increases. Corresponding to $\phi = 0^\circ$, the inclined load becomes the normal load, and hence, the plot of shear stress starts from zero, and thereafter, it exhibits extremely small values in comparison with the other curves. Figure 13 is plotted to show the distribution of temperature field against distance x for four different values of ϕ . The behavior of temperature field is almost similar for $\phi = 30^\circ, 60^\circ$ and 90° , whereas the solution curve corresponding to $\phi = 0^\circ$ shows reverse pattern. Also, inclination angle has an increasing effect on the distribution of temperature field.

7.4 Effect of time

Figures 14, 15, 16 and 17 represent the distributions of normal displacement, normal stress, shear stress and temperature, respectively, against the location x for three distinct instants of time t (0.01, 0.05 and 0.10). A careful view of the profiles shows that time is having a noticeable increasing effect on the distributions of these physical fields throughout the whole domain.

8 Concluding remarks

The main purpose of current study is to present a new mathematical model for an initially stressed fiber-reinforced orthotropic thermoelastic medium. The method of normal mode analysis is used to study the current problem which proves to be a quite successful technique to handle such type of problems. This technique gives exact results without any pre-assumed constraints on the actual physical field quantities existing in the governing field equations of the considered problem. The above analysis gives the following conclusions

- The normal displacement, normal stress, shear stress and temperature field are highly affected by the parameters of fiber reinforcement. The magnitude of normal displacement and temperature field in orthotropic medium is higher in comparison with transversely isotropic and isotropic media while normal stress and shear stress show different behaviors.
- Significant impact of Green–Naghdi theories (type III and type II) is observed on all the field variables. In the context of GN II theory, the magnitude of temperature field is higher than that of the same field variable under GN III theory, while normal displacement exhibits the reverse behavior and normal stress exhibits a different behaviors. Green–Naghdi theories have no effect on the profile of shear stress.

- In the presence of initial stress, the normal displacement and temperature field have higher magnitude in comparison with the same in the absence of initial stress while normal stress and shear stress show different behavior.
- All the field variables show similar pattern for different values of angle of inclination ϕ of the applied mechanical load except for $\phi = 0^\circ$. The magnitudes of all the field variables increase as the angle of inclination increases except the normal stress.
- Displacement component u , normal stress σ_{xx} , shear stress σ_{xy} and temperature distribution θ show almost similar pattern for distinct instants of time t , and an increase in the value of time causes an increase in the magnitudes of all the physical fields, which is quite clear from the plots.
- All the physical quantities satisfy the considered boundary conditions of the problem.

References

1. Mallick PK (2007) Applications of fiber-reinforced composites. Fiber-reinforced composites: materials manufacturing and design. CRC Press, Taylor and Francis Group, London, Dekker Mechanical Engineering Series, pp 1–20
2. Abbas IA (2011) A two-dimensional problem for a fiber-reinforced anisotropic thermoelastic half-space with energy dissipation. *Sadhana* 36:411–423
3. Hashin Z, Rosen WB (1964) The elastic moduli of fiber-reinforced materials. *J Appl Mech* 31:223–232
4. Pipkin AC (1973) Finite deformations of ideal fiber-reinforced composites. In: Sendeckyj GP (ed) *Composites materials*, vol 2. Academic, New York, pp 251–308
5. Rogers TG (1975) Anisotropic elastic and plastic materials. In: Thoft-Christensen P (ed) *Continuum mechanics aspects of geodynamics and rock fracture mechanics*. Reidel, Dordrecht, pp 177–200
6. Belfield AJ, Rogers TG, Spencer AJM (1983) Stress in elastic plates reinforced by fiber lying in concentric circles. *J Mech Phys Solid* 31:25–54
7. Singh B (2006) Wave propagation in thermally conducting linear fiber-reinforced composite materials. *Arch Appl Mech* 75:513–520
8. Othman MIA, Lotfy K (2013) The effect of magnetic field and rotation of the 2-D problem of a fiber-reinforced thermoelastic under three theories with influence of gravity. *Mech Mater* 60:129–143
9. Kalkal KK, Sheokand SK, Deswal S (2018) Two-dimensional problem of fiber-reinforced thermo-diffusive half-space with four relaxation times. *Mech Time Depend Mater* 23:443–463
10. Deswal S, Sheokand SK, Kalkal KK (2019) Thermo-diffusive interactions in a fiber-reinforced elastic medium with gravity and initial stress. *J Braz Soc Mech Sci Eng* 41:1–11
11. Biot M (1956) Thermoelasticity and irreversible thermodynamics. *J Appl Phys* 27:240–253
12. Lord HW, Shulman YA (1967) A generalized dynamical theory of thermoelasticity. *J Mech Phys Solid* 15:299–309
13. Green AE, Lindsay KA (1972) Thermoelasticity. *J Elast* 2:1–7
14. Green AE, Naghdi PM (1991) A re-examination of basic postulates of thermomechanics. *Proc R Soc Lond Ser A* 432:171–194
15. Green AE, Naghdi PM (1992) On undamped heat waves in an elastic solid. *J Therm Stress* 432:253–264
16. Green AE, Naghdi PM (1993) Thermoelasticity without energy dissipation. *J Elast* 31:189–208
17. Biot MA (1965) *Mechanics of incremental deformation*. Wiley, New York
18. Montanaro A (1999) On singular surfaces in isotropic linear thermoelasticity with initial stress. *J Acoust Soc Am* 106:1586–1588
19. Ailawalia P, Singh N (2009) Effect of rotation in a generalized thermoelastic medium with hydrostatic initial stress subjected to ramp type heating and loading. *Int J Thermophys* 30:2078–2097
20. Abbas IA, Abd-Alla AN (2011) Effect of initial stress on a fiber-reinforced anisotropic thermoelastic thick plate. *Int J Thermophys* 32:1098–1110
21. Kumar R, Garg SK, Ahuja S (2015) Wave propagation in fiber-reinforced transversely isotropic thermoelastic media with initial stress at the boundary surface. *J Solid Mech* 7:223–238
22. Deswal S, Kalkal KK, Sheoran SS (2016) Axi-symmetric generalized thermoelastic diffusion problem with two-temperature and initial stress under fractional order heat conduction. *Physica B* 496:57–68
23. Khan AA, Afzal A (2018) Influence of initial stress and gravity on refraction and reflection of SV wave at interface between two viscoelastic liquid under three thermoelastic theories. *J Braz Soc Mech Sci Eng* 40:1–13
24. Deswal S, Punia BS, Kalkal KK (2018) Reflection of plane waves at the initially stressed surface of a fiber-reinforced thermoelastic half space with temperature dependent properties. *Int J Mech Mater Des* 15:159–173
25. Spencer AJM (1984) *Continuum theory of the mechanics of fibre-reinforced composites*. Springer. ISBN 978-3-7091-4336-0
26. Ezzat MA, Awad ES (2009) Micropolar generalized magneto-thermoelasticity with modified Ohm's and Fourier's laws. *J Math Anal Appl* 353:99–113
27. Othman MIA, Atwa SY (2013) Two-dimensional problem of a fiber-reinforced anisotropic thermoelastic medium, comparison with the Green–Naghdi theory. *Comput Math Model* 24:307–325
28. Abbas IA, Abd-Alla AN, Othman MIA (2011) Generalized magneto-thermoelasticity in a fiber-reinforced anisotropic half-space. *Int J Thermophys* 32:1071–1085

Publisher's Note Springer Nature remains neutral with regard to jurisdictional claims in published maps and institutional affiliations.